The Astrophysical Journal, 667:275–287, 2007 September 20

PHOTOIONIZATION RATES IN CLUMPY MOLECULAR CLOUDS

T. J. Bethell,[1] E. G. Zweibel,[2] and Pak Shing Li[3]
Received 2006 August 16; accepted 2007 May 23

ABSTRACT

We present calculations of the continuum ultraviolet radiation field (91.2 nm $< \lambda <$ 550 nm) penetrating both uniform and clumpy (3D turbulent supersonic magnetohydrodynamic) starless molecular gas layers. We find that despite the self-shielding of clumps, pristine (i.e., unreddened) radiation penetrates deeply both the cloud's *volume* and its *mass*, resulting in a brighter and bluer intracloud radiation field compared to that in an equivalent uniform cloud. Motivated by these results, we construct and test a toy model ray-tracing scheme for the radiative transfer that fits the UV-visible spectral range with a three-parameter function. We calculate the photoionization rates, Γ, of the elements C, Na, Mg, Si, S, and Fe as functions of the visual extinction A_V along lines of sight. Typically, the difference in $\Gamma(A_V)$ between the clumpy and uniform clouds increases to orders of magnitude at even modest extinctions ($A_V \sim 2$). Photoionization in the clumpy model extends 2–3 times deeper than in the uniform case, and it dominates cosmic-ray ionization throughout almost the entire volume. We encapsulate these average results in a parameterized form appropriate for when an approximate treatment of the effects of clumpiness is desired. However, the large point-to-point variance in this behavior suggests that uncertainties may arise when using mean values to model particular lines of sight in detail. Ideally, these new results would be used in conjunction with established results for homogeneous clouds in order to span a range of behavior that arises due to cloud inhomogeneities. We briefly explore the importance of the adopted dust properties, characterized by the selective extinction R_V and the scattering parameter g. We find that the UV field is considerably less sensitive to these dust properties in clumpy clouds, emphasizing the preeminence of geometry.

Subject headings: astrochemistry — ISM: clouds — ISM: structure — radiative transfer

1. INTRODUCTION

Ultraviolet (UV) radiation plays an important physical role in much of the interstellar medium, through processes such as photoelectric heating (Bakes & Tielens 1994), grain charging (Weingartner & Draine 2001), photoionization of metals (Roberge et al. 1981), and photodissociation of molecules (Hollenbach & Tielens 1997). Regions in which the UV field plays a dominant role are termed photodissociation or photon-dominated regions (PDRs; Hollenbach & Tielens 1999). Importantly, these PDRs are considered to be ubiquitous in the Galaxy, especially in regions of enhanced UV radiation fields, and they regulate the physical state of large quantities of molecular material. For example, the importance of UV radiation in interstellar chemistry and in determining the ionization fraction $x_e = n_e/n_{\rm H}$ (which affects the coupling of the gas with the magnetic field) must be understood before the picture of star formation is complete (McKee 1989; Padoan et al. 2004; Mouschovias et al. 2006).

All of the aforementioned physical processes require some knowledge of the *ambient* UV field, typically involving some form of radiative transfer. For many astrophysical processes the role of scattering cannot be ignored a priori, complicating the radiative transfer considerably. As a result, much of the previous work has been based on radiative transfer results for simple geometries and uniform distributions of material (Flannery et al. 1980).

There is abundant observational evidence indicating that molecular clouds are in fact highly inhomogeneous in their internal structures on all scales (Perault et al. 1985; Deshpande 2000; Heiles 1997; Faison & Goss 2001). While clumpiness has long been invoked to successfully interpret observations that are inexplicable in a solely homogeneous framework (Martin et al. 1984; Stutzki et al. 1988; Meixner & Tielens 1993; Jansen et al. 1995; Schnee et al. 2006), the inclusion of inhomogeneities in numerical models has also underlined the difficulties of extracting robust and unambiguous information from such data (Mathis et al. 2002; Wood et al. 2005). Only relatively recently have the computational tools become sufficiently powerful and accessible to allow highly detailed modeling of clumpy regions (Witt & Gordon 1996; Bethell et al. 2004, hereafter B04; Juvela 2005). A variety of novel semianalytic methods have also been developed for solving the clumpy radiative transfer problem (Boissé 1990; Hobson & Scheuer 1993; Hobson & Padman 1993; Hegmann & Kegel 1996), although these often suffer from unphysical mathematical restrictions such as requiring isotropic dust scattering or a spatially random clumpiness. Dust scattering is generally considered to be highly forward-throwing in the UV (Lillie & Witt 1976; Sujatha et al. 2005), and the clumping of dense interstellar material is considered to be hierarchical, not simply random (Stutzki & Güsten 1990; Kramer et al. 1998). Nevertheless, these analytical methods have shed much light on the fundamental nature of the problem.

In brief, a point internal to a clumpy cloud may be bathed in intense radiation penetrating along a few optically thin lines of sight, whereas observing that point along a random line of sight might give the impression that it is deeply embedded, for example. The concept of a visual extinction, A_V, calculated in the traditional way and that characterizes the radiative transfer has little meaning in the case of a clumpy distribution, as the photons that reach a point in the cloud have not experienced the same extinction suggested by calculating A_V along a given line of sight from the edge to this point. While this may seem a trivial point to make, it is absolutely central to the issue of radiative transfer. The observational characterization of a cloud's structure is often limited to a line-of-sight extinction, A_V, which as an integral quantity says

[1] Department of Astronomy, University of Michigan, Ann Arbor, MI 48109; tbethell@umich.edu.
[2] Department of Astronomy, University of Wisconsin, Madison, WI 53706.
[3] Theoretical Astrophysics Center, University of California, Berkeley, CA 94720.

almost nothing explicit about the interior three-dimensional (3D) extinction structure of the cloud. Only by applying very basic assumptions about geometry can A_V be put to any practical use within the framework of radiative transfer calculations. As has been shown in B04 and in other similar works, the enhanced porosity of "realistically" clumpy clouds greatly encourages radiation to penetrate the cloud's volume, which is generally well illuminated by the V band (0.55 μm) relative to a homogeneous cloud of similar mass. On the other hand, one cannot necessarily make this claim for the clumpy *mass*. In their clumpy, turbulent cloud, B04 found the highly self-shielding clumps to be statistically less well illuminated in the visual spectral band. A complementary feature arising in clumpy clouds is an enhancement in the blueness of the penetrating radiation field, attributable to almost pristine interstellar radiation passing through optically thin windows. In other words, as we go to shorter wavelengths, the "blueness effect" will increasingly mitigate the "mass is dark effect." One of the purposes of this paper is to demonstrate that the blueness effect dominates in the UV and that both the clumpy mass and volume are both statistically well illuminated.

The effect of "realistic" inhomogeneities on the radiative transfer of photoionizing radiation clearly deserves a detailed investigation. In this paper we explore how clumpy 3D structures in the dense ISM affect the radiative transfer of ionizing ultraviolet radiation ($\lambda > 91.2$ nm). To achieve this goal we construct a clumpy planar cloud from a magnetohydrodynamic simulation, which we then bathe in the ultraviolet interstellar radiation field, solving the radiative transfer using a Monte Carlo method. At every stage we compare these results with those for a uniform cloud of the same mean density and optical depth. The greatly enhanced mean photoionization rates in the clumpy cloud are shown to follow the parameterized form traditionally used for uniform clouds, as is predicted by previous theoretical work. The subsequent role played by our photoionization rates in the chemistry of dense clumpy regions, placing an emphasis on the ionization fraction x_e, will be explored in a companion paper (Bethell et al. 2007).

The paper proceeds with § 2, in which we introduce the uniform and clumpy planar clouds. In § 3 we describe the methods used to (1) calculate numerically the penetration of an isotropic and homogeneous external interstellar radiation field (ISRF) into the model molecular clouds, (2) perform the parametric modeling of the intracloud spectra, and (3) parameterize the ionization rates of the elements C, Na, Mg, Si, S, and Fe. In § 3.2 we discuss the results of our radiative transfer calculations and some of the more interesting statistics of the radiation field. In § 3.3 we apply the spectral modeling and test the applicability of its underlying assumptions.

Section 4 presents the photoionization rate calculations for our clouds. We analyze the results as a function of extinction along lines of sight. Effective γ-values and related quantities are calculated for the clumpy clouds that could be used in existing photochemical models. We conclude this section with a brief exploration of the effects of changing the dust properties. The implications of our main results are discussed in § 5.

2. THE MODEL CLOUDS

The existence of clumps on scales far below the Jeans scale suggests a nongravitational origin for much of the structure. The supersonic line widths detected in all but the smallest molecular clouds (Zuckerman & Evans 1974; Evans 1999) are a natural source of clumpy structure. Indeed, magnetized supersonic turbulence driven on large scales and cascading to smaller scales seems to offer a plausible explanation for the complex clumps, filaments, and sheets often seen in observations (Elmegreen & Scalo 2004; Mac Low & Klessen 2004; Beresnyak et al. 2005).

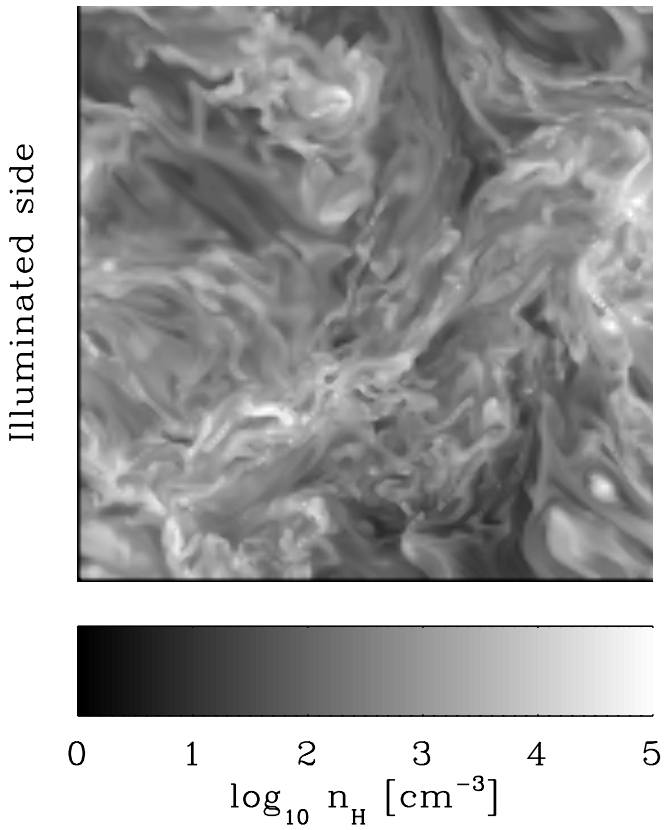

FIG. 1.—Slice of the hydrogen density continuum of the clumpy cloud. This slice is referenced elsewhere in the paper when we show the morphology of other physical quantities. Note that this is not a column density map.

We base our clumpy cloud model on a 512^3 uniform cubical grid simulation of self-gravitating, driven MHD turbulence by Li et al. (2004). The simulations are described fully in that paper. The data cube we use is a snapshot chosen at 0.8 free-fall times after starting the gravitational collapse. We choose this snapshot for its high degree of clumpiness and its statistical homogeneity (it exhibits no obvious voids that would offset the distribution of matter). A slice through the clumpy cloud is shown in Figure 1. The mean density is taken to be $\langle n_{\rm H} \rangle = 10^3$ cm^{-3}, typical of molecular clouds. The density distribution is well described by a lognormal distribution (see Fig. 2); the lowest values of $n_{\rm H}$, of a few per cm^{-3}, are associated with the interclump medium, and the largest values, $n_{\rm H} \sim 10^7$ cm^{-3}, with the centers of self-gravitating cores. The fractions of the cloud mass associated with gas above densities of 10^3, 10^4, and 10^5 cm^{-3} are 0.77, 0.25, and 0.02, respectively. The cores in our cloud do not significantly skew the density normalization.

The turbulent clouds possess periodic boundaries, which allows them to be stacked infinitely to form a clumpy slab. We use such a construction to model the skin of a larger molecular cloud, and we note that the planar geometry is prevalent in similar work found in the literature (Roberge et al. 1981).

As shown in B04, the differences in these simulations due to their different Mach numbers and plasma beta values do not have an effect on the radiative transfer greater than that of the intrinsic temporal variability in these models, so we restrict our studies to a single model.

In order to assess the effects of clumpiness, we carry out parallel calculations for infinite homogeneous slabs of the same mean

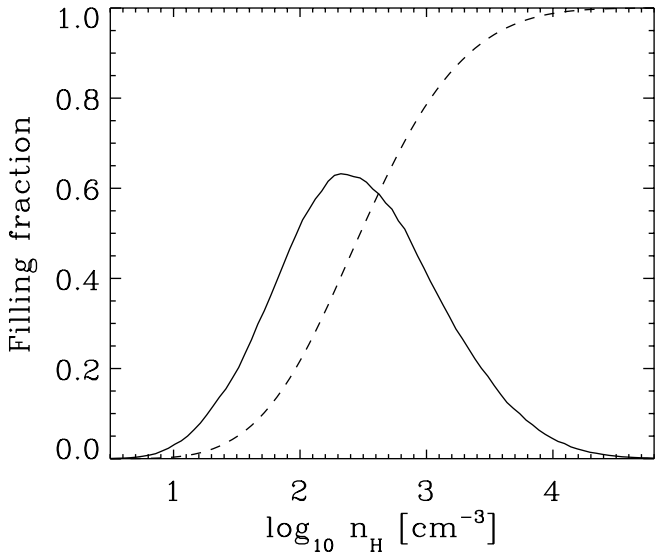

FIG. 2.—Statistics of the density continuum in our clumpy model. The solid line indicates the volume filling fraction of the clumpy cloud occupied by material with (logarithmic) density $\log_{10} n_{\rm H}$, per unit $\log_{10} n_{\rm H}$. The dashed line shows the corresponding cumulative distribution. The median density is approximately 400 cm^{-3}.

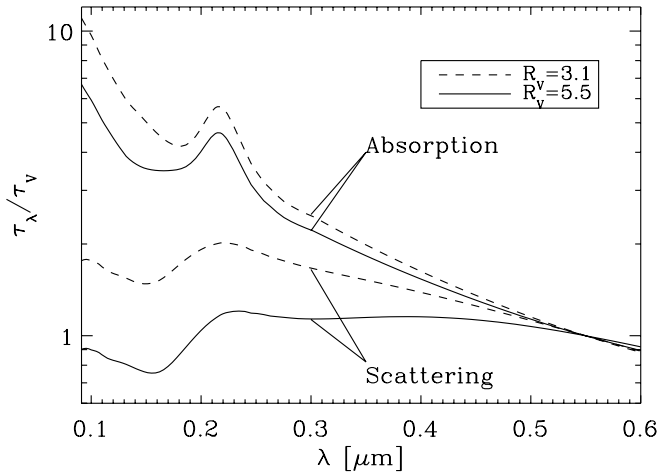

FIG. 3.—Absorption and scattering cross sections for both types of dust (R_V = 3.1 and 5.5), shown normalized to their V-band values.

density $\langle n_{\rm H}\rangle$ and physical size L (and thus the same mass), such that their visual optical depth, looking perpendicularly into the skin, is $\langle \tau_V \rangle = 0.93 A_V = 10$. We assume spatially uniform dust properties and a constant gas-to-dust ratio. Depending on the dust type chosen, the visual optical depth of a sight line is related to its column density by $\tau_V \sim 0.6 \times 10^{-21} N_{\rm H}$. Computations on the homogeneous slab are carried out on an a grid identical to that used for the turbulent slab.

3. THE INTRACLOUD UV SPECTRUM

The transfer of radiation is through coherent, anisotropic scattering by interstellar dust particles. Under these conditions, the radiative transfer equation can be written as the sum of two terms, the first term describing the removal of photons from a beam, $I(\boldsymbol{k})$, and the second term giving the redistribution of photons scattered from other directions $\boldsymbol{k}' \neq \boldsymbol{k}$ into $\boldsymbol{k}$. The radiative transfer equation in its entirety is given by

$$\frac{dI(\boldsymbol{k})}{ds} = -(\sigma_{\rm abs} + \sigma_{\rm sca}) n_{\rm H} I(\boldsymbol{k}) + \int d\Omega(\boldsymbol{k}')\, R(\boldsymbol{k}', \boldsymbol{k}) \sigma_{\rm sca} n_{\rm H} I(\boldsymbol{k}'). \quad (1)$$

The quantities $\sigma_{\rm abs}$ and $\sigma_{\rm sca}$ are, respectively, the absorption and scattering cross sections due to dust per hydrogen nucleus, and $R(\boldsymbol{k}', \boldsymbol{k})$ is the redistribution function, reflecting the probability that a photon is scattered from direction $\boldsymbol{k}'$ into direction $\boldsymbol{k}$.

We use two populations of dust grains for which the detailed optical properties have been calculated by Weingartner & Draine (2001) and Draine (2003).[4] The extinction curves of these populations are distinguished observationally by their total-to-selective extinction ratios $R_V \equiv A_V/E(B-V)$, and we select populations for which $R_V = 3.1$ and 5.5, which are appropriate for "diffuse" and "outer cloud" interstellar dust, respectively (Cardelli et al. 1989; Mathis 1990). An increase in R_V represents a relative reduction of UV extinction and is often associated with the removal of small grains by either grain mantle growth or grain coagulation. While our clumpy cloud represents a dense region (where $R_V \sim 5.5$ would be appropriate), it also is presumably in contact with the diffuse ISM (where $R_V \sim 3$). In order to avoid introducing an additional complication, we assume a default value of $R_V \sim 5.5$. In reality, high- and low-density regions in close proximity may contain different dust populations. Furthermore, as pointed out in the original work of Cardelli et al. (1989), variations about these mean R_V laws are readily observed in the ISM. The wavelength dependences of $\sigma_{\rm abs}$ and $\sigma_{\rm sca}$ are shown in Figure 3. The redistribution function we use is from Henyey & Greenstein (1941), although modifications to this are also possible (Draine 2003; Witt 1977). The Henyey-Greenstein function $R(\boldsymbol{k}', \boldsymbol{k})$ involves a scattering parameter $g \equiv \langle \cos\theta \rangle$, where θ is the scattering angle. From this definition it is clear that g lies in the range $[-1, 1]$, where $g = -1$ corresponds to pure backscattering, $g = 0$ to isotropic scattering, and $g = 1$ to pure forward-scattering. Typically g is taken to be largely forward-throwing; i.e., $g = 0.5$–0.75 in the visible-UV wavelength range (Witt et al. 1990; Sasseen & Deharveng 1996; Calzetti et al. 1995), although there is a considerable uncertainty in this quantity (Sujatha et al. 2005).

Dust is not the only significant source of UV opacity. The Lyman-Werner bands of H_2 remove a considerable fraction of the flux in the wavelength range [0.0912, 0.111] μm. The exact calculation is prohibitively complicated in the context of this paper; however, an approximate upper limit to the fraction of radiation lost to Lyman-Werner line absorption may be on the order of a few tens of percent (Abgrall et al. 1992; Fig. 13 of Draine & Bertoldi 1996). The relevant photoionization regime of carbon, which has a photoionization threshold wavelength of $\lambda_{\rm th} \sim 0.111$ μm, lies almost exactly on top of the Lyman-Werner bands. The carbon ionization rate may therefore be diminished by a factor of a few, the exact value depending on details of the cloud geometry and the H_2 line transfer calculations (Spaans 1996). For species with larger photoionization threshold wavelengths, the effect of the Lyman-Werner bands is proportionally less significant. The typical dust extinction curve rises steeply toward the UV, ensuring that much of the radiation contributing to ionization is found near the threshold wavelength. We therefore ignore the Lyman-Werner bands, concentrating on dust opacity instead, and recognize that the ionization rates will, to varying degrees, be somewhat overestimated. Nevertheless, the comparison between clumpy and uniform clouds, which represents the main focus of this paper, will still be a useful one.

[4] For tabulated data, see http://www.astro.princeton.edu/~draine.

The radiative transfer equation (eq. [1]) is a boundary value problem. In our case the $z = 0$ face is the surface of the skin and is illuminated by an isotropic interstellar radiation field (ISRF). Radiation may leave but not enter the $z = L$ face; thus, we neglect the small amount of backscattered radiation emanating from the bulk of the molecular cloud beyond our skin. This also assumes that there is no radiation traveling through the hypothetical molecular cloud from its far side, requiring that the total cloud is considerably optically thicker than our skin (which is consistent with the idea of a skin). Accordingly, we enforce periodic boundary conditions in the x- and y-directions. In this way we construct an imaginary skin out of our turbulent MHD cube that extends infinitely and periodically in the x- and y-directions and is illuminated isotropically on one face ($z = 0$) only.

3.1. *Reverse Monte Carlo Radiative Transfer*

The turbulent clouds are sufficiently inhomogeneous and structured that the detailed penetration of the external radiation field must be calculated using a numerical method. We employ the reverse Monte Carlo (RMC) radiative transfer code described in B04; we give here only a brief overview. To calculate the relative mean intensity J_λ at position x, the code constructs a large number of "reverse trajectories" coupling x to the ISRF. The trajectories are composed of contiguous segments, the length of segment i being a probabilistic sampling of the optical depth for pure scattering $\tau_{i,\mathrm{sca}}$ that is then rendered as a distance s_i in physical space. The corresponding pure absorption opacity $\tau_{i,\mathrm{abs}}$ along the segment is then $\tau_{i,\mathrm{sca}}(1-\omega)/\omega$, where ω is the albedo. The angles between trajectory segments are found by sampling probabilistically from the Henyey-Greenstein redistribution function. A large number of trajectories are initiated isotropically about point x until the trajectories form a representative, probabilistic representation of all possible trajectories linking x to the ISRF. The generation of trajectories depends only on pure scattering, while the ultimate attrition of photons along their lengths depends only on their total pure absorption optical depths (pure scattering is conservative). Care should be taken in properly interpreting the physical meaning of the "first" and "last" trajectory segments, although these considerations do not introduce any additional technical difficulties.

One notable advantage of the RMC method is that it enables the user to efficiently obtain a uniform signal-to-noise ratio throughout the cloud, which is of particular importance in self-shielding clumps, where much of the mass resides, and which are not necessarily well explored by photons in forward Monte Carlo (FMC) schemes. Because trajectories must be recalculated for each point, the method is perhaps best suited to calculating J_λ at a subset of points. We typically calculate J_λ at every other grid point; thus, our original density cube of 256^3 cells yields a J_λ cube of 128^3 cells, although it is worth noting that the underlying radiative transfer is still computed using the higher resolution. Furthermore, the RMC code, despite being three-dimensional, naturally allows one-dimensional and two-dimensional (2D) calculations to be performed efficiently; one simply places sources of reverse trajectories along the lines (one dimension) or surfaces (two dimensions) of interest. While the potential of the RMC method has been somewhat underutilized, we feel it prudent to comment on its limitations. Without modification, the RMC method can be relatively inefficient when the source of radiation is localized, or when one wishes to calculate the radiation field throughout large volumes. It is therefore unsurprising that the most efficient scheme has elements of both the forward and reverse methods. For example, the reprocessing by dust of UV and visible stellar photons into infrared photons, and the reheating of dust by this dust emission, is often treated in an FMC code. However, depending on the problem, the visible and UV photon transfer may best be treated in an RMC framework, while the infrared emission is treated with an FMC method. The natural output of our code is the unitless *relative* mean intensity J_λ, the mean intensity at wavelength λ inside the cloud divided by the ISRF value I_λ.

In principle, the procedure described above must be followed for every wavelength of interest. In § 3.3 and in the Appendix we describe a method for fitting the spectrum at each point in space with a function of three parameters. The fits are accurate enough to reconstruct the continuum spectrum at arbitrarily high wavelength resolution by calculating ray paths at only ~5 wavelengths. This greatly reduces the computational time required for the calculation and provides a conceptual framework for understanding which factors control the radiation field.

3.2. *Results*

In one-dimensional homogeneous clouds, the extinction from the cloud's edge, $A_V \propto n_{\mathrm{H}} z$, uniquely determines the mean intensity spectrum at a point for a given set of dust properties (ω, g, R_V, etc.). In this way J_λ can be related to the observable A_V; that is, there exists a function $J_\lambda(n_{\mathrm{H}}, z)$. Flannery et al. (1980) showed that for a homogeneous semi-infinite half-space illuminated on one side by an isotropic radiation field, the relative mean intensity J_λ at wavelength λ and visual optical depth τ_V from the surface can be written in the form

$$J_\lambda = \sum A_n \exp(-K_n \tau_V), \tag{2}$$

where A_n and K_n are constants to be determined by the particular problem. In particular, K_n depends on the extinction curve τ_λ/τ_V, the albedo ω, and the scattering phase function parameter g. In the asymptotic limit of large τ_V, equation (2) is dominated by the smallest K_n value (referred to here as K_{asym}), so J_λ is simply exponentially attenuated with depth.

The possibility that a function also exists, albeit empirically, for a clumpy cloud motivates us to consider the uniqueness of spectra at points that have identical, well-defined physical quantities n_{H} and z. Figure 4 shows the spectra in a narrow range of densities and physical depths. The large variance in the spectra at these physically similar points suggests that no useful empirical function $J_\lambda(n_{\mathrm{H}}, z)$ exists for our clumpy clouds. This is not the same as saying that $J_\lambda(n_{\mathrm{H}}, z)$ is independent of extinction, of course; it is just that the mean extinction at a point is relatively independent of depth.

B04 claimed that in clumpy *spheres*, the mass is statistically less well illuminated by V-band radiation than in the uniform case. That is, the global distribution of mass as a function of J_V peaked at a lower value of J_V in the clumpy models. However, when the mass-weighted J_V was calculated in concentric shells, it was shown that this effect is largely confined to the regions in close proximity to the cloud surface, in which, due to spherical divergence, much of the mass resides. The interior of their clumpy sphere was brightly illuminated in the V band (in both mass- and volume-weighted senses; see Fig. 6 in B04). In this paper we consider slabs (which of course do not exhibit spherical divergence); thus, the interior is more evenly represented in these statistical considerations.

The distributions of mass and volume with J_V are shown in Figure 5. Within our clumpy skin, both the mass and volume distributions are broadly peaked. As previously discussed, J_V varies exponentially with depth in the uniform cloud according to the

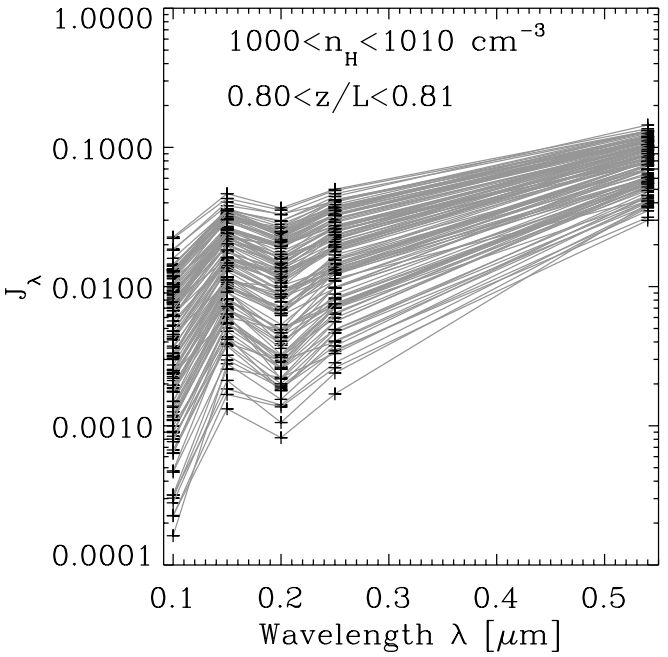

FIG. 4.—Spectral data from our RMC calculations, taken from points in the clumpy cloud with similar values of density and depth position z/L, where L is the total physical depth of the skin.

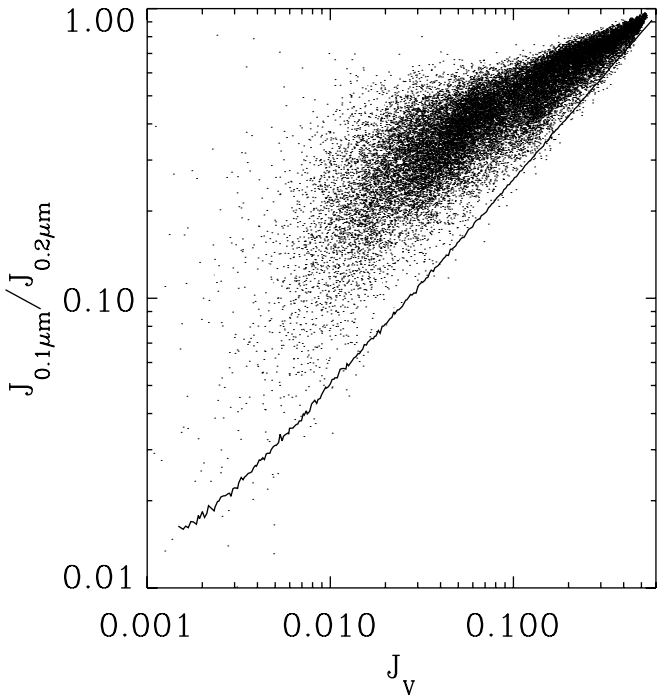

FIG. 6.—Scatter plot of the UV color $J_{0.1\ \mu m}/J_{0.2\ \mu m}$ as a function of J_V in the clumpy cloud. The solid line shows the result for the uniform cloud. Note that these colors are relative to the corresponding ISRF color.

asymptotic form given by equation (2). In this case the mass is guaranteed to be distributed uniformly (ignoring binning noise) among the *logarithmic* bins in Figure 5.[5]

The clumpy cloud exhibits a considerably bluer UV spectrum, as shown in Figure 6, where we have plotted the colors of a randomly chosen subset of points. Note the large scatter in the clumpy cloud, indicating clearly that there is no one-to-one correspondence between *V*-band intensity and color (i.e., spectral slope).

The distribution of mass and volume with UV color is shown in Figure 7. The corresponding clumpy result shows that statistically, both the mass and the volume are illuminated by bluer radiation. Furthermore, the low-density material sees a bluer UV radiation field than do the high-density regions, which is consistent

[5] The truncation of this distribution at small J_V is due to the finite depth of our skin; the neglect of backscattered radiation entering the inner boundary is responsible for the non-abruptness of the truncation.

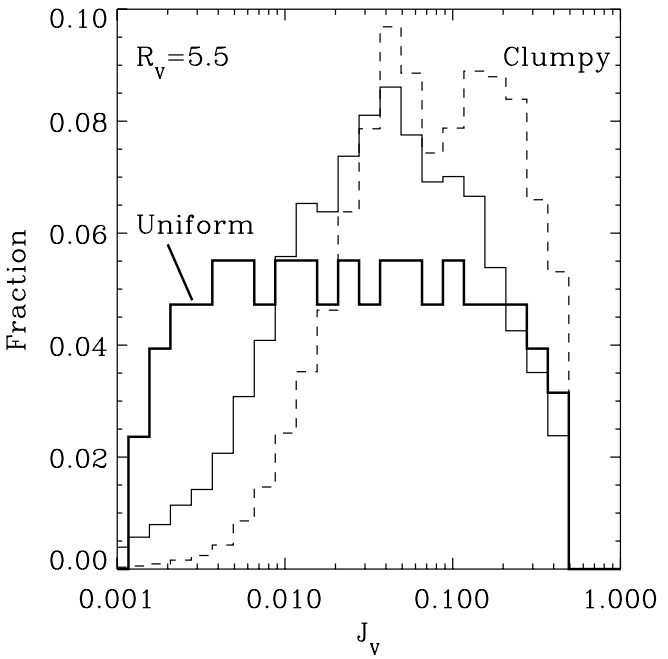

FIG. 5.—Mass (*solid line*) and volume (*dashed line*) distributions as a function of *V*-band intensity J_V in the clumpy (*thin lines*) and uniform (*thick solid line*) clouds.

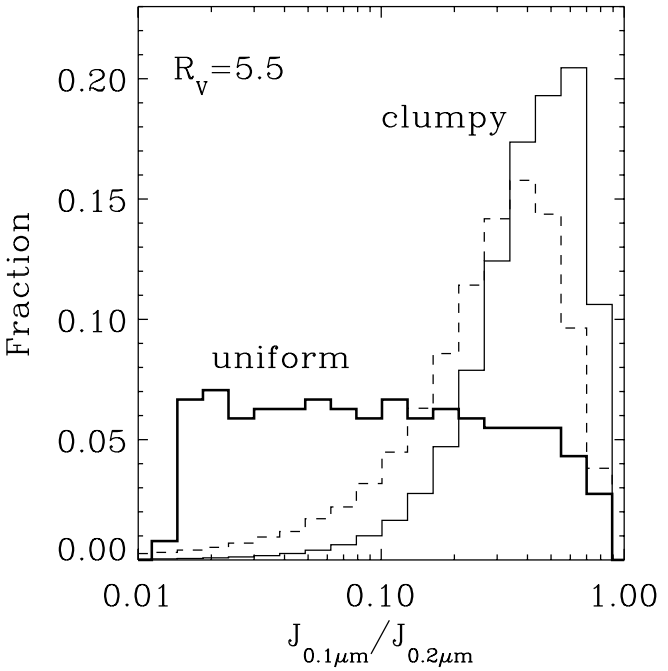

FIG. 7.—Histograms of the mass (*solid line*) and volume (*dashed line*) fractions of the clumpy cloud with color $J_{0.1\ \mu m}/J_{0.2\ \mu m}$. The thick solid line shows the result for the uniform cloud.

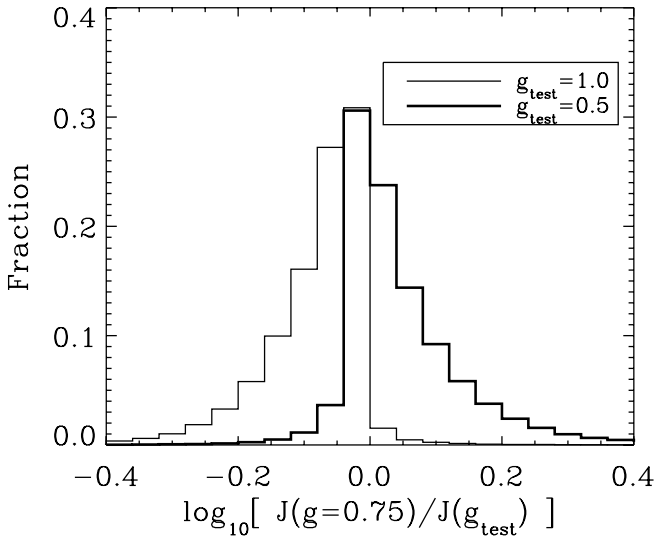

FIG. 8.—Comparison between three RMC calculations that differ in the scattering parameter g, but are otherwise identical.

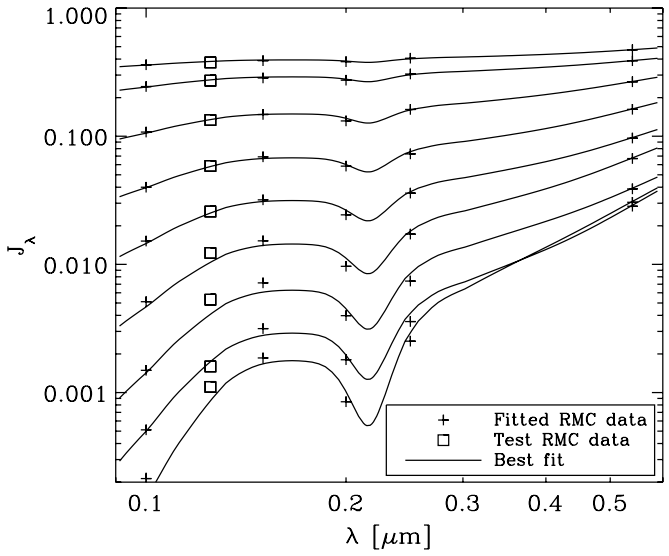

FIG. 9.—Test of the spectral fit. The spectra (*solid lines*) are fitted to the RMC data (*plus signs*). Independent RMC calculations at 0.125 μm (*squares*) are used to test the predictions of the model spectra. Each spectrum represents a random position in the clumpy cloud.

with clumps experiencing additional self-shielding (reddening of the radiation field).

3.3. *The Spectral Fitting Method*

The underlying idea behind the spectral fitting method is that the radiation field at any point in the cloud depends approximately on three parameters: the fraction of the sky obscured by clumps, the optical depth of the clumps, and a local component of extinction related to the immediate environment (see the Appendix). This representation is meaningful only if the contribution of scattered light is relatively low, a point that we establish in § 3.3.1. We developed a fitting method for two reasons: to reduce the computational time required to calculate the radiation spectrum, and to see whether the radiation field can be deduced from morphological features without actually solving the radiative transfer equation. We were successful in the first quest, but not in the second, at least for clumpy clouds of the type considered here. As a glance at Figure 1 suggests, the sky visible from any typical point is too complex to be parameterized by three variables.

3.3.1. *The Importance of Scattering*

To show conclusively that the effects of scattering can largely be ignored, we compute J_λ at $\lambda = 0.125$ μm throughout our clumpy cloud for a range of scattering parameters: $g = 0.5$, 0.75 (believed to be the physical value), and 1.0. At $\lambda = 0.125$ μm the clumpy cloud has an average optical depth of $10\tau_{0.125\ \mu\mathrm{m}}/\tau_V \sim 50$. The value of g in the visible-UV wavelength range is not expected to drop much below $g = 0.5$, while a value of $g = 1.0$ suppresses the effects of scattering altogether. In Figure 8 we plot histograms of the discrepancies between $J(g = 0.75)$ and $J(g = 0.5,\ 1.0)$. In general, increasing g increases J; forward-throwing scattering events cause less deviation in a photon's path, the photon's total path length between two points is shorter, and the subsequent optical depth of pure absorption along the trajectory's length is less. In uniform planar clouds the effect of changing g is appreciable (see Fig. 4 in Flannery et al. 1980) and can account for changes in J of factors of a few. Despite the large average UV optical depth of the clumpy cloud, the value of g does not seem to affect the results strongly. For the majority of points, varying the value of g by ± 0.25 about the physical value changes J by less than a factor of 2. There are a few places in the cloud where increasing g *decreases* J; these points are typically in the shadows of clumps where only scattered photons can reach.

It is worth noting that in the case of $g = 1$ the photon trajectories are straight lines and the radiative transfer can be solved using the conceptually simple and computationally expedient ray-tracing method, which is precisely what the RMC method becomes.

3.3.2. *The Spectral Fits*

Having established in § 3.3.1 that the scattered flux is not the dominant source of radiation, we can more confidently approach modeling the spectra with a toy model. The parameters are found using a modified version of the IDL curve-fitting procedure CURVEFIT. The wavelengths at which we perform the fitting are $\lambda = 0.10$, 0.15, 0.20, 0.25, and 0.54 μm. While a different set of wavelengths may yield different and possibly more constrained fits, we adopt these values for practical convenience. The fitting function explained in the Appendix, once expanded, contains two terms, the first containing only the "local" parameters Ω and $\tau_{V,l}$. In the case in which the first term dominates, the fit becomes degenerate with respect to $\tau_{V,g}$, resulting in a two-parameter function that is insensitive to the fiducial optical depths of the clumps.

To test the accuracy of the spectral fit, we perform an additional RMC calculation at 0.125 μm, a wavelength that lies among the threshold wavelengths for photoionization, and compare these "test data" to the predictions of our fitted spectra. A random sample of spectra from our clumpy cloud is shown in Figure 9. It can be seen that the fitting function generally succeeds in fitting the five data points and, to a lesser degree, predicts the nonfitted test data at 0.125 μm. The fitted spectra lack the curvature of the true spectra in the UV. Nevertheless, the agreement is generally good, and it is rarely worse than that depicted in Figure 9, even at large attenuations, where one might expect our basic assumptions to falter. The quantitative discrepancy between test data and fitted values throughout our clumpy cloud is shown in Figure 10 as a histogram. The spectral fit at 0.125 μm systematically underestimates the true value, but it remains within 0.1 dex of the true value throughout 90% of the cloud.

The wavelengths used for the fitting were chosen somewhat subjectively, producing the most consistently reliable fits. Other

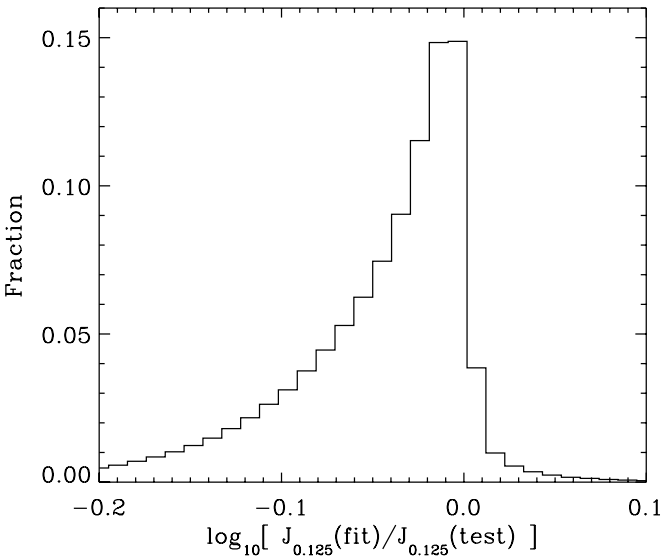

FIG. 10.—Volume fraction histogram of the discrepancy between the spectral fit and the test data (the true RMC value) in the clumpy cloud for $R_V = 5.5$ dust.

wavelengths were considered, including 0.22 μm, where we find the well-known "bump" in the extinction curve. In general, we found that fitting this point compromised the fit at shorter wavelengths, the accuracy of which is of primary concern. This is a weakness of the underlying assumptions of the fitting function, revealing that not all wavelengths can be fitted equally well without introducing further parameters into the fitting formula. Understandably, the fitting method is less successful when applied to the uniform cloud, as the underlying physical construction of the method is no longer applicable. We find that it still succeeds to a depth of $A_V \sim 5$. Regardless, here the spectral fitting is not necessarily advantageous, since the uniform cloud requires only a one-dimensional calculation, and as such the spectra can be built directly and quickly from RMC calculations.

4. IONIZATION RATES

The direct cosmic-ray ionization rate $\zeta \sim 10^{-17}$ s^{-1} is often taken as the basal H_2 ionization rate in molecular clouds, becoming the dominant source of ionization wherever large extinctions prevail. Cosmic rays can also ionize metals indirectly by exciting Lyman-Werner emission of H_2, consisting of photons with sufficient energy to photoionize most metal atoms (Prasad & Tarafdar 1983). Because these photons are produced in the abundant H_2 reservoir, they represent to a metal atom a more intense source of ionization than that due to direct cosmic-ray ionization. These rates are typically on the order of 10^{-14} s^{-1}, although this number is subject to large uncertainties. This is then the basal cosmic-ray–induced ionization rate for the metals. There has been much discussion over the homogeneity of ζ both among and within molecular clouds (Williams et al. 1998; Caselli & Walmsley 2001; Padoan et al. 2004). Strong evidence for variable values of ζ could imply local sources of cosmic rays, complex magnetic topology, or local variations in the cosmic-ray diffusion rate, so it is important for cosmic-ray and galactic magnetic field astrophysics to pin this down.

The photoionization rate of a species with cross section $\sigma_{\rm ph}(\lambda)$ is given by

$$\Gamma = \frac{4\pi}{hc} \int \lambda \sigma_{\rm ph}(\lambda) J_\lambda I_\lambda \, d\lambda \ {\rm s}^{-1}, \tag{3}$$

TABLE 1
PHOTOIONIZATION RATES Γ^0 (10^{-10} s^{-1}) IN THE UNATTENUATED ISRF

Reaction	α (UMIST)	MMP	Draine (1978)
$C + h\nu \rightarrow C^+ + e^-$	3.0	2.7	3.6
$Na + h\nu \rightarrow Na^+ + e^-$	0.15	0.089	0.13
$Mg + h\nu \rightarrow Mg^+ + e^-$	0.79	0.53	0.82
$Si + h\nu \rightarrow Si^+ + e^-$	31	27	42
$S + h\nu \rightarrow S^+ + e^-$	5.9	4.9	6.5
$Fe + h\nu \rightarrow Fe^+ + e^-$	2.8	1.7	2.6

where h is Planck's constant, c is the speed of light, and I_λ is the mean specific intensity of the unattenuated ISRF. For consistency, we adopt the ISRF of Draine (1978), although we also use the ISRF of Mathis et al. (1983, hereafter MMP) to briefly test the importance of the choice of the ISRF (see § 4.1). The photoionization cross sections are taken from the analytical fits of Verner et al. (1996).

Much of the previous work on photoionization has concentrated on mathematically one-dimensional objects (e.g., spheres and slabs). The subsequent inclusion of these results as photoreaction rate coefficients Γ in the widely used UMIST[6] astrochemical database (see also Lee et al. [1996] for an alternative) has led to the following parameterization for general photoreaction rates:

$$\Gamma = \alpha \exp(-\gamma A_V). \tag{4}$$

The quantity α is meant to represent the photoionization rate in the unattenuated ISRF, Γ^0, and therefore depends on the spectral form of the adopted ISRF. Crudely speaking, γ represents the enhancement of the UV extinction relative to that at visual wavelengths, and as such it depends on both the details of the opacity source (the dust opacity, albedo, and scattering properties) and the cloud geometry. As we noted in equation (2), the exponential form of equation (4) is reminiscent of the large-A_V limit of the solution to the one-dimensional radiative transfer equation in planar geometry. In this limit, the parameter α would be analogous to the corresponding A_n value ($A_{\rm asym}$); however, it is often more closely identified with the full $\sum A_n$, which causes equation (4) to overestimate the ionization rate in the asymptotic limit by a considerable factor, often in excess of an order of magnitude. To account for this error, we still use $\alpha \equiv \Gamma^0$, but include an additional prefactor χ that represents the fraction of Γ^0 carried by the asymptotic term. One of our main goals is to evaluate the ionization rates as functions of visual extinction and provide empirical parameter values that can be used in existing astrochemical calculations. In our notation we have

$$\Gamma/\Gamma^0 = \chi \exp(-\gamma A_V). \tag{5}$$

The parameter α in the UMIST database would then be replaced with $\chi\Gamma^0$. For $\tau_V < 1$ the asymptotic solution should not be used at all; instead, a partial or full expansion of the type in equation (2) is preferred (Roberge et al. 1981).

4.1. *Results*

The calculated ionization rates of atomic species exposed to the unattenuated MMP and Draine (1978) ISRFs are shown in Table 1, along with the α-values from the UMIST database. The UMIST values were calculated for the Draine ISRF, which we use

[6] The UMIST database is available online at http://www.udfa.net.

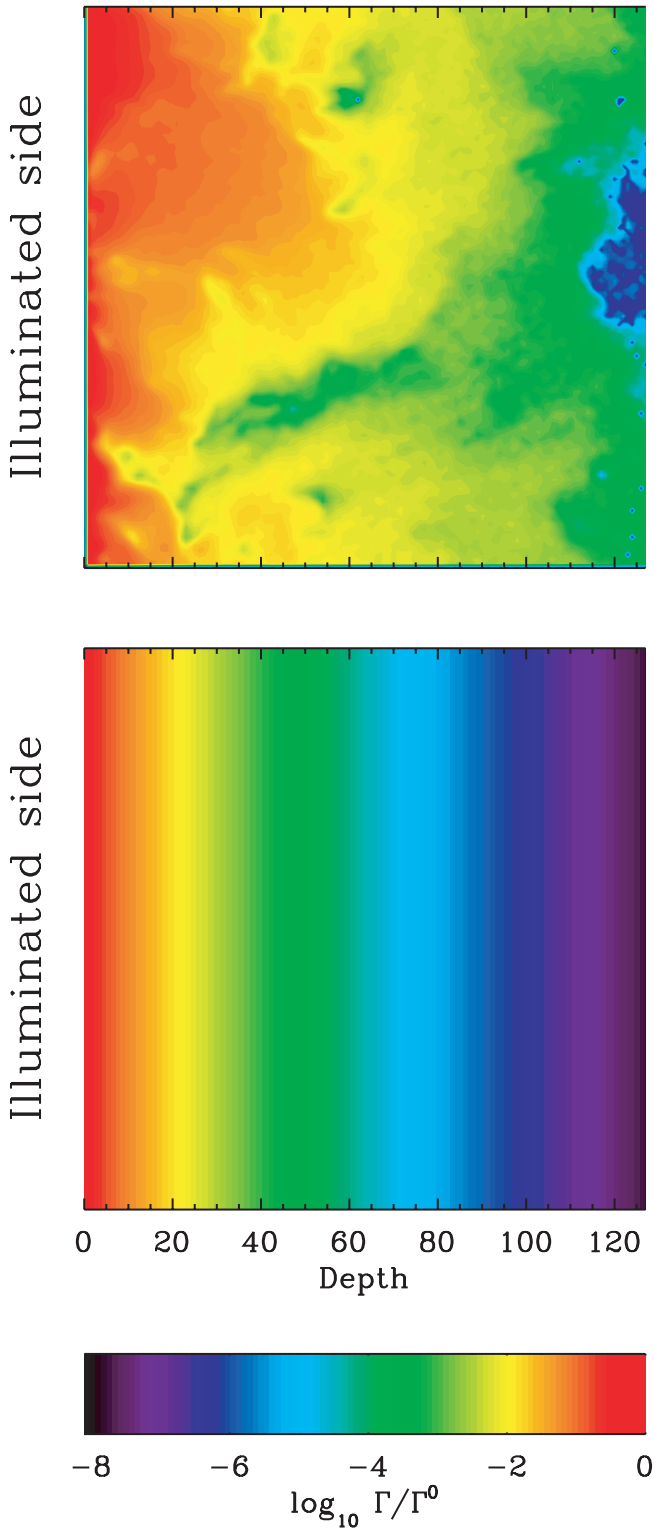

FIG. 11.—Slice of the relative carbon ionization rate Γ/Γ^0 in the clumpy cloud (*top*) and the uniform cloud (*bottom*). The depth is given in units of cells from the illuminated face, with the total depth corresponding to $L = 4.75$ pc. This slice corresponds to the density slice shown in Fig. 1.

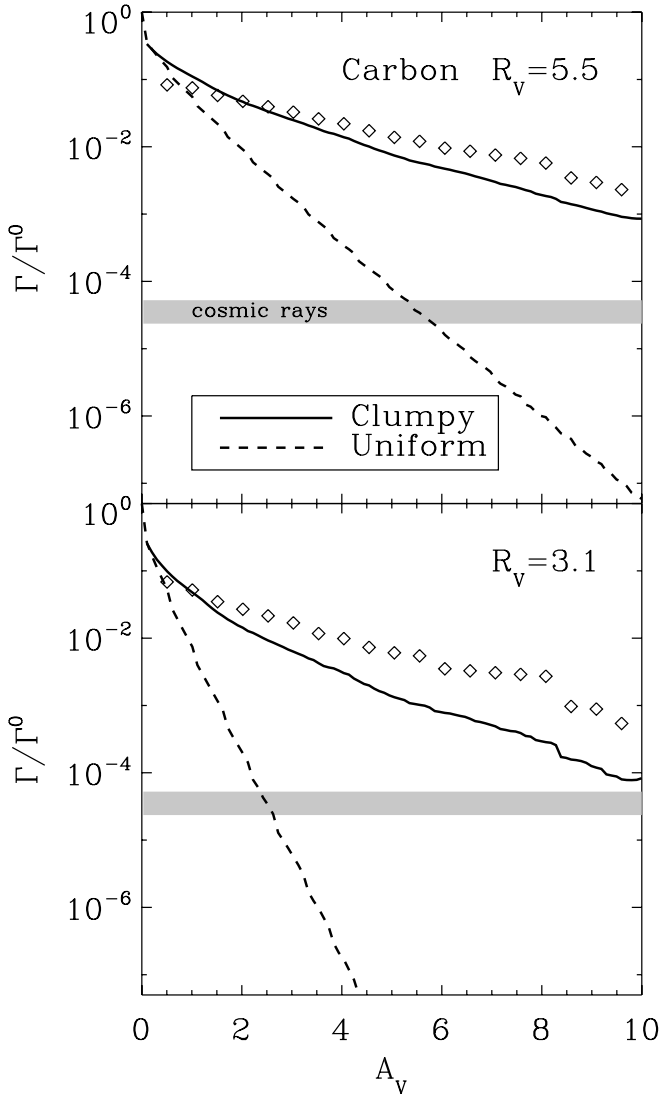

FIG. 12.—Mass-averaged photoionization rate of carbon as a function of A_V along selected lines of sight entering the illuminated face of the cloud. The chosen lines of sight have a total extinction through the skin of $A_V \geq 10$. The diamonds indicate the magnitude of the rms scatter about the mean for the clumpy cloud. This scatter is larger in magnitude than the mean, which indicates that for a given A_V, there exists a nonnegligible amount of mass that is intensely illuminated. The top and bottom panels differ only in the adopted R_V value used. The gray region represents an estimate of the cosmic-ray–induced ionization rate taken from the UMIST database.

in our calculations. However, some divergence from the UMIST results is expected, since we use the more recent photoionization cross sections of Verner et al. (1996). Reassuringly, our Draine ISRF values generally agree best with the corresponding UMIST α-values. The MMP field produces ionization rates that are typically lower than those we obtain from the Draine ISRF, although they agree to within a factor of 2. In the relevant UV spectral regime, the Draine field can be about 1.6 times stronger than the MMP field (see Fig. 2 in Evans et al. 2001), and this explains much of the Draine-MMP discrepancy. The ionization rates cited in UMIST for the elements C, Mg, Si, and S fall within the Draine-MMP discrepancy; however, the UMIST values for Na and Fe are slightly larger than their respective Draine values.

Slices through the carbon ionization rate in the uniform and clumpy clouds, for which $R_V = 5.5$, are shown in Figure 11. In the clumpy cloud there is a weak trend of decreasing photoionization with increasing physical depth, although the effect of self-shielding by clumps is clearly evident when compared with the density slice in Figure 1.

4.1.1. *Ionization Rate versus A_V: γ-Values*

In Figure 12 we plot the mass-averaged ionization rate of carbon as a function of A_V along lines of sight into both the clumpy

TABLE 2
VALUES OF γ

REACTION	UMIST	$R_V = 3.1$ Uniform	$R_V = 3.1$ Clumpy	$R_V = 5.5$ Uniform	$R_V = 5.5$ Clumpy
$C + h\nu \rightarrow C^+ + e^-$	3.0	3.5	0.65	1.5	0.51
$Na + h\nu \rightarrow Na^+ + e^-$	1.8	2.1	0.54	1.2	0.44
$Mg + h\nu \rightarrow Mg^+ + e^-$	1.7	2.1	0.53	1.2	0.43
$Si + h\nu \rightarrow Si^+ + e^-$	1.9	2.3	0.55	1.2	0.44
$S + h\nu \rightarrow S^+ + e^-$	2.6	3.2	0.63	1.4	0.49
$Fe + h\nu \rightarrow Fe^+ + e^-$	1.9	2.3	0.55	1.2	0.44

NOTE.—The variability in γ arising from using different orientations of the same clumpy cloud is typically ± 0.03, or less than 10%.

and uniform clouds. We clearly see a large enhancement in ionization rate compared to that of the uniform cloud, as well as a large scatter. Fortunately, the variation of Γ with A_V is indeed almost exponential, facilitating the parameterization described in § 4. For $2 < A_V < 8$ we fit equation (5) to these curves for each of the photoionization processes considered. The values of γ are given in Table 2, and the values of χ in Table 3. The clumpy γ-values are relatively constant among the different species and are less than the corresponding values for a uniform cloud by factors of 2–5. We attribute this to the markedly bluer radiation fields found in clumpy clouds (see Fig. 6). Table 3 measures the validity of the single exponential fit to J_λ with depth in a cloud. Not surprisingly, the fit is worse in clumpy than in uniform clouds, because the system is not plane-stratified.

We also see in Figure 12 a large rms scatter about the mean Γ/Γ^0. At small A_V the standard deviation is less than the mean, simply because the ionization rate is approaching its maximum possible value; i.e., that at the cloud edge. At moderate to large A_V the scatter exceeds the mean, indicative of a small fraction of the cloud mass that is extremely well illuminated. Looking at the morphology of the cloud, it becomes clear that much of this behavior is due to the differences between the interiors and surfaces of clumps that have an appreciable optical depth. In magnitude this scatter is comparable to that seen in the calculations of Boissé (1990), who argues that it arises partially as a result of the reduced role of scattering, which would otherwise tend to smooth the radiation field.

If we take a more global view of the distribution of ionization rate with mass and volume, we find the result shown in Figure 13. Here we see that while the mass in the uniform cloud is distributed evenly among the logarithmic bins of ionization rate, both the mass and volume fractions are strongly peaked at large ionization rates for the clumpy cloud. Unsurprisingly, in a globally averaged sense, the ionization rate anticorrelates with density in the clumpy cloud.

TABLE 3
VALUES OF χ (10^{-2})

REACTION	$R_V = 3.1$ Uniform	$R_V = 3.1$ Clumpy	$R_V = 5.5$ Uniform	$R_V = 5.5$ Clumpy
$C + h\nu \rightarrow C^+ + e^-$	20	4.5	17	11
$Na + h\nu \rightarrow Na^+ + e^-$	14	6.7	22	15
$Mg + h\nu \rightarrow Mg^+ + e^-$	22	8.2	28	17
$Si + h\nu \rightarrow Si^+ + e^-$	22	6.7	25	15
$S + h\nu \rightarrow S^+ + e^-$	18	4.5	18	12
$Fe + h\nu \rightarrow Fe^+ + e^-$	18	6.7	22	15

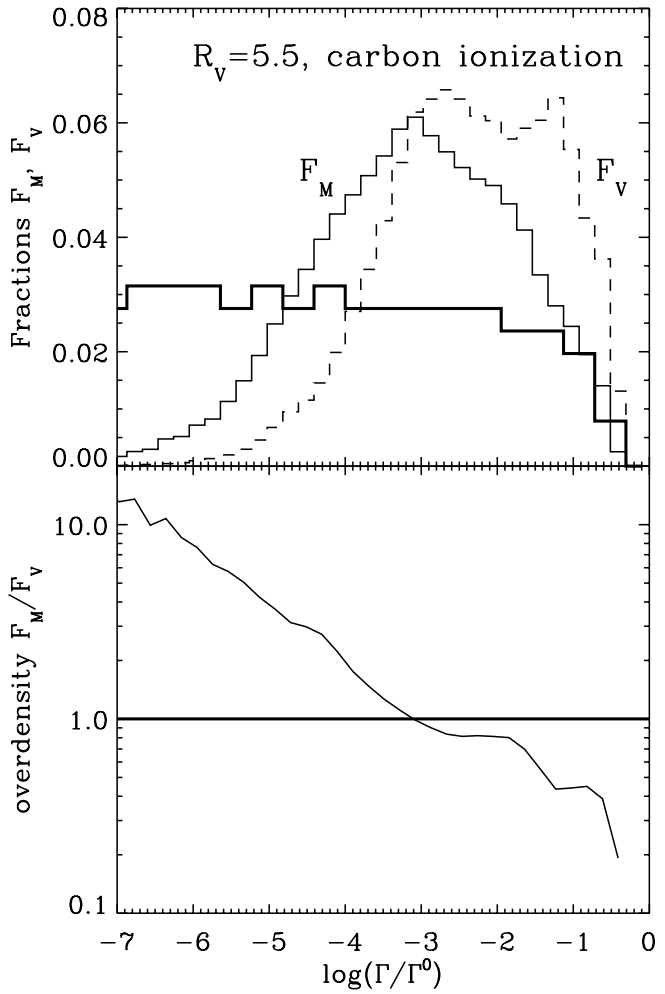

FIG. 13.—*Top*: Fractions of mass (F_M; *solid line*) and volume (F_V; *dashed line*) with carbon ionization rate Γ/Γ^0 for the clumpy cloud. The thick solid line represents the same for the uniform cloud. *Bottom*: Corresponding average overdensity (the density of a sample divided by the mean density of the entire cloud; i.e., F_M/F_V) of material as a function of the ionization rate.

In Figure 14 we consider the fraction of carbon mass dominated by photoionization (as opposed to cosmic-ray ionization) as a function of A_V. In the uniform case A_V is the sole determining variable, and consequently there is a well-defined depth ($A_V \sim 5.5$ for $R_V = 5.5$ dust) at which photoionization ceases to play the dominant role. In the clumpy case all of the carbon is dominated by photoionization down to only $A_V \sim 3$, at which point cosmic-ray ionization increasingly (if slowly) becomes significant. Clearly, this intermingling of material dominated by photoionization and cosmic-ray ionization should be addressed when modeling such regions. For example, one might attempt to model the ionization state of the gas as a function of A_V more realistically by applying our radiative transfer results (using the γ-parameterization) to some decreasing fraction f of mass given by Figure 14, while the remaining fraction $1 - f$ is taken to be cosmic-ray–ionized.

4.1.2. *Influence of R_V*

In the previous sections we have established that a clumpy geometry allows a few optically thin lines of sight to dominate the intracloud radiation field. The radiation flowing in these optically thin directions exhibits only a weak signature of dust extinction. We might therefore expect our clumpy results to show only a weak dependence on R_V. In uniform clouds the effect of

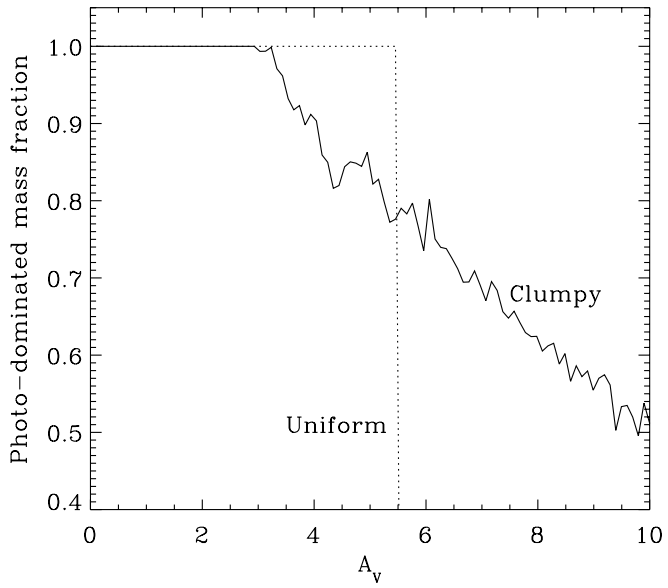

FIG. 14.—Fraction of carbon mass for which the photoionization rate exceeds the cosmic-ray ionization rate, shown as a function of A_V for the clumpy (*solid line*) and uniform (*dotted line*) clouds.

changing R_V is known to be large (Mathis 1990; Cecchi-Pestellini et al. 1995). In the bottom panel of Figure 12 we recompute $\Gamma(A_V)$ for $R_V = 3.1$, the "diffuse" dust value, and find that it causes a much more rapid extinction of UV radiation in the uniform model, but enhances the attenuation only very slightly in the clumpy cloud. The resulting values of γ are tabulated in Table 2 for comparison. The uniform result is highly sensitive to the larger $\tau_{\rm UV}/\tau_V$ values of $R_V = 3.1$ dust. This is a persistent trend; as one decreases R_V, the discrepancy between clumpy and uniform cloud models becomes increasingly large. It is worth noting that the UMIST values, which were compiled from a number of sources, lie in between the $R_V = 3.1$ and 5.5 values for our uniform clouds.

5. SUMMARY AND DISCUSSION

Using a reverse Monte Carlo radiative transfer code and spectral modeling, we have calculated the intracloud UV field and subsequent photoionization rates in clumpy and uniform clouds. Our primary goals were to understand the effects of clumpiness and dust properties on the radiative transfer and photoionization rates. Our results on radiative transfer are consistent with those of Boissé (1990), who found order-of-magnitude enhancements of the radiation field in clumpy clouds. While his calculation was restricted to somewhat unphysical density structures and isotropic dust scattering, we have used a single, more realistic density continuum and anisotropically scattering dust properties.

The principal results of our calculations are these:

1. Compared to a uniform cloud of similar mass, we have found that the external UV field penetrates efficiently both the mass and volume of our clumpy cloud skin, resulting in a more intense and bluer intracloud spectrum (Figs. 5 and 6). If PDRs are defined as regions where UV photons play a significant role in determining the physical conditions (Hollenbach & Tielens 1997), then clumpy clouds even more extended than ours should also be considered PDRs.

2. The UV radiation spectrum at most points can be fitted to better than a factor of 2 by a function of three variables: the clump covering fraction, clump extinction, and extinction by the immediate environment (see Figs. 15, 9, and 10). Spectral fitting substantially reduces the computational time needed to reconstruct the radiation spectrum, but fitting parameters cannot be found from cloud morphology alone; it is necessary to solve the radiative transfer equation.

3. In clumpy clouds the ionization rates of various metals decrease very slowly with depth into the cloud, enhanced by 2 orders of magnitude at values of A_V of only $\sim$4. Due to the blueness of the UV field, variations with depth of the photoionization rates of elements C, Na, Mg, Si, S, and Fe appear to behave similarly in the clumpy cloud, in contrast to the uniform cloud, in which carbon ionization tends to be relatively concentrated in the outer regions.

4. Although a large variance is present in the data, we were able to parameterize the ionization rates in the conventional form found in the UMIST chemistry database (Table 2). We added a correction to the single exponential fit law parameterized by χ (see Table 3). It is our hope that these parameters will prove useful for calculations in which the mean effects of clumpiness need to be considered, if only at a crude level. Due to the large scatter, we must emphasize that the parameterized fits are most suitable for modeling *gross* properties.

5. The important role played by geometry diminishes that played by dust properties in clumpy clouds. Our results for the *uniform* cloud, adopting two rather different dust populations characterized by $R_V = 3.1$ and 5.5, support previous work that emphasizes the importance of the dust properties (e.g., Cecchi-Pestellini et al. 1995). However, in the clumpy context the ionization rates are almost entirely insensitive to R_V (see Fig. 12).

Based on these results, a preliminary discussion of the implications and consequences is in order.

The penetration of radiation into clumpy clouds is so efficient that even for the mean Galactic interstellar radiation field, its effect on photoelectric heating and dust charging remain important at greater depths than predicted for uniform clouds. Furthermore, photoionization dominates cosmic-ray ionization for most of the clumpy mass, even beyond $A_V = 10$. However, cosmic-ray–dominated regions first make an appearance at lower extinctions, $A_V \sim 3$, compared to $A_V \sim 5.5$ for the uniform cloud. While calculations of the ionization fraction x_e and associated ions are left for a future paper (Bethell et al. 2007), it is clear that x_e will be increased considerably, largely exacerbating the problem of decoupling the magnetic field from the gas prior to star formation. Using arguments based on the ionization rates in smooth cores, McKee (1989) concluded that photoionization dominates cosmic-ray ionization down to depths of $A_V \sim 4$, which constituted the bulk of molecular material in his models. In light of our results, photoionization may play a significant role at $A_V \sim 10$, provided that the cores are sufficiently clumpy. In the case of carbon, we neglected the role played by the H_2 Lyman-Werner opacity, which in a homogeneous cloud may reduce the carbon photoionization rates by a factor of a few. Since we have established the critical role played by the relatively low optical depth lines of sight, it seems reasonable that the effects of the Lyman-Werner band may be mitigated, at least in these low-density regions. Indeed, if these channels have sufficiently low densities and experience large UV fluxes, then the molecular hydrogen itself may be almost entirely photodissociated, reducing the H_2 opacity even further. Molecular hydrogen self-shields against this photodissociation at a column density of H_2 of around 10^{15} cm^{-2}, although this value depends on factors such as the density and UV flux (Lee et al. 1996). Of course, much of the mass resides in clumps, which will be almost completely molecular. A self-consistent treatment of the transition between atomic and molecular hydrogen requires a coupling of molecular hydrogen formation on grains and radiative transfer

through the Lyman-Werner bands. To make matters worse, since molecular hydrogen can potentially self-shield over extremely small spatial scales, the radiative transfer requires some sort of adaptive mesh to resolve small transitions. Errors in the method propagate readily throughout the calculation, since the radiative transfer depends on the molecular abundance and vice versa. Unsurprisingly, such calculations are currently limited to one dimension and can only be extended to higher dimensions by simplifying the radiative transfer (e.g., Spaans & Neufeld 1997).

Chemical analyses of star-forming cores that assume that photoionization processes play a negligible role in the core evolution (i.e., that they are "dark") may need to be reconsidered in the context of a broader, clumpy cloud structure (Padoan et al. 2004). The temporal variability of the UV field may also prove to be an important consideration. The UV field is dominated by direct flux streaming through a few relatively transparent windows, which themselves are formed and destroyed on short timescales ($\lesssim 10^5$ yr) by the turbulent and bulk motions of clumps inside the cloud. In the context of nonlinear chemical processes, these intermittent periods of UV illumination are sufficiently frequent to enhance photodestruction and ionization processes while stifling the onset of a rich "late-time" chemistry. For example, the recovery and photoionization of C from CO could explain the larger C/CO and C^+/CO ratios seen in M17, where both density inhomogeneities and an enhanced UV field are presumably present. On the other hand, the periodic compression of gas due to supersonic turbulent motions enhances UV self-shielding, providing a safe environment for the production of complex organic molecules (Chieze et al. 1991). Garrod et al. (2005) presented the first detailed time-dependent chemical models of cores undergoing compression and rarefaction, with a turnover time on the order of 1 Myr. They found significant enhancements of important molecules such as CO, H_2O, CH_4, and NH_3; however, their treatment did not explore the effects of a time-varying ambient radiation field. B04 and this paper show that large spatial variations exist in the intracloud radiation field, which presumably translate to large temporal variations as the structure evolves.

It may be best to use these parameterized values in conjunction with those for the uniform cloud. Together they form a pair of geometries that bracket many intermediate situations. The tabulated values for the clumpy case are likely to be model-dependent, although we lack the time and resources to perform a comprehensive study of this dependence. Thus, we are merely presenting the values for a cloud that we deem to be reasonably realistic and that might prove a useful guide for those reluctant or unable to perform expensive radiative transfer calculations of their own. Within the parameter space of our "realistic" turbulent MHD simulations, we do not expect large excursions from these tabulated values, primarily because the radiation fields calculated in B04 were found to be largely insensitive to the physical properties of the underlying models (Mach number, magnetic field strength, etc.).

One important aspect of these results that is somewhat more difficult to address is the large scatter observed about the average trends. The traditional parameterization that we continue to advocate does not and cannot address this issue. A small fraction of extremely well illuminated mass may become conspicuous when folded into complex, nonlinear chemical networks. In molecular clouds the cosmic-ray– and photoionization-driven chemistries depend largely on the production of H_3^+ and metal ions, respectively. The chemical evolutions that follow are understandably quite different. To varying degrees, a line of sight will include regions driven by each mechanism. These regions produce their own chemical signatures, complicating the interpretation of molecular observations. Furthermore, the large ionization fraction in well-illuminated regions will tend to tie this mass to the underlying magnetic field. The subsequent suppression of ambipolar drift will likely play a significant role in the overall evolution of the cloud and its magnetic field. We will investigate these issues more deeply in a future paper.

Finally, the dominant role of low-extinction lines of sight in determining the cloud radiation field reduces the sensitivity of the intracloud radiation field on the adopted dust model. This then further complicates the already difficult task of determining the basic optical properties of dust (ω and g) by modeling observations of inhomogeneous objects such as reflection nebulae (Witt et al. 1990; Code & Whitney 1995; Mathis et al. 2002; and for a review, see Gordon 2004).

We are happy to acknowledge useful discussions with John Mathis, Mark Neyrinck, and especially Fabian Heitsch, who also assisted us greatly in the use of his cloud models. Material support was provided by NSF and NASA grants to the University of Wisconsin, as well as the UW Graduate School.

APPENDIX

SPECTRAL MODELING

The semianalytic works of Boissé (1990) and Hobson & Scheuer (1993) identify the *unscattered* intensity as the dominant component of the internal radiation field. This corresponds to the predominance of the first term in equation (1) with the scattering opacity removed. Motivated by this, Hobson & Scheuer (1993) constructed a simple model based on a "clump covering factor," the fraction of sky obscured by clumps. This simple model qualitatively reproduced the results of their more detailed calculation. Boissé also noted that his average clumpy results could be reproduced by using *effective* optical properties with a uniform medium. This result, despite the unphysical aspects of the work, suggests that the various types of parameterization used for uniform clouds could also be applied to the clumpy case.

The neglect of scattering is most appropriate when the flux is dominated by a few optically thin lines of sight. This requirement is relaxed somewhat if the scattering function of the dust is highly forward-throwing, in which case few photons are scattering into or out of a beam regardless of the number of scattering events.[7] Given the large range of column densities in our clumpy cloud and the largely forward-throwing scattering properties of our dust, it seems intuitively reasonable to describe the radiative transfer in terms of the following phenomena:

Shadowing.— An observer (situated at a point inside the cloud) sees relatively opaque objects blocking light, with little or no wavelength dependence when the covering structures have sharp, well-defined boundaries (i.e., large density gradients around clumps).

[7] In the case of forward-throwing scattering ($g = 1$), the redistribution function in eq. (1) becomes a delta function, the integral over which produces a source term that exactly cancels the effects of the sink term due to scattering of the beam.

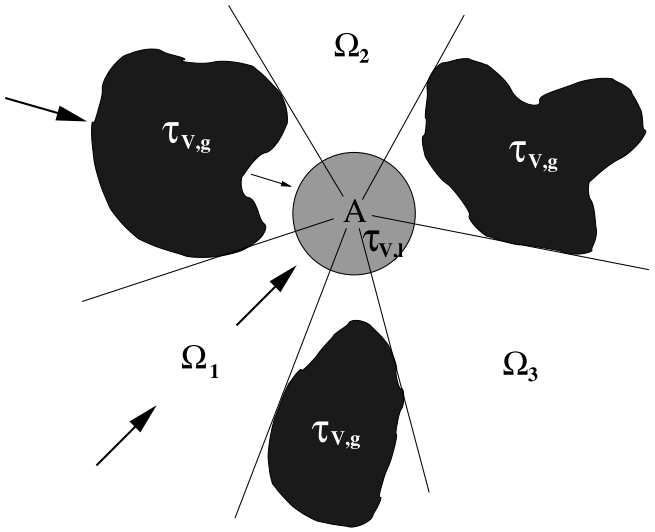

FIG. 15.—Cartoon of the toy model for the radiative transfer used to formulate our spectral modeling method. An observer situated at point A experiences an isotropic local optical depth $\tau_{V,l}$, beyond which there are high-extinction clumps (possibly superposed in projection) of some fiducial optical depth $\tau_{V,g}$. The fractions of sky unobscured by clumps (i.e., unshadowed) are denoted by Ω_i. The arrows simply represent imaginary beams of photons entering the cloud from the ISRF for which scattering is assumed to play a negligible role.

The view from within the clumpy cloud then appears structurally similar at all wavelengths. In this case the role of shadowing can be expressed as a single parameter, Ω, defined as the fraction of *unobscured* sky.

Extinction.— The wavelength-dependent removal of photons from a ray leaves an imprint of the extinction curve on the intracloud spectrum. In an astrophysical context, this typically leads to reddening.

An illustrative cartoon of the toy model is shown in Figure 15, and its physical interpretation is as follows. If a fraction $\Omega = \sum \Omega_i$ of an observer's sky has a relatively low column density, then the remaining fraction $1 - \Omega$ can be said to be passing only highly attenuated radiation (shadowing) with a characteristic optical depth $\tau_{V,g}$. Both Ω and $\tau_{V,g}$ are essentially *global* (i.e., are not strongly dependent on local conditions), so to ensure that clumps can self-shield, we introduce a characteristic *local* optical depth $\tau_{V,l}$ that applies to every direction in the observer's entire sky. Conceptually, $\tau_{V,l}$ could also be partially attributed to the nonlocal low-density material that fills the interclump volume. The most important assumptions of the model are that Ω is wavelength-independent and that scattering events are sufficiently infrequent or forward-throwing that they do not appreciably remove photons from a beam. The model predicts the spectra seen by the observer at position A thusly:

$$J_\lambda = \exp\left(-\frac{\tau_\lambda^{\rm abs}}{\tau_V^{\rm abs}}\tau_{V,l}\right)\left[\Omega + (1-\Omega)\exp\left(-\frac{\tau_\lambda^{\rm abs}}{\tau_V^{\rm abs}}\tau_{V,g}\right)\right]. \quad \text{(A1)}$$

The equation is written in this form to emphasize that we find the V-band optical depths $\tau_{V,l}$ and $\tau_{V,g}$, which, within the scope of the toy model, are related to the optical depths at other wavelengths by the *pure absorption* extinction curve $\tau_\lambda^{\rm abs}/\tau_V^{\rm abs}$. The steps involved in the spectral fitting are as follows:

1. Using the radiative transfer code, compute J_λ at five wavelengths (we use $\lambda = 0.1$, 0.15, 0.2, 0.25, and 0.54 μm).
2. Compute $\tau_\lambda^{\rm abs}/\tau_V^{\rm abs}$, the normalized pure absorption part of the extinction curve from which the values of J_λ were computed (see Fig. 3).
3. Using $\tau_\lambda^{\rm abs}/\tau_V^{\rm abs}$ and equation (A1), find the three parameters Ω, $\tau_{V,l}$, and $\tau_{V,g}$ for each point in the cloud.
4. Test the fit by computing, say, $J_{0.125\,\mu{\rm m}}$ with the RMC code and comparing this with the prediction of the spectral fit.

The benefits of such a model are twofold; first, it allows one to infer the radiation field at all relevant wavelengths from calculations performed at only a handful of wavelengths, thus saving a considerable amount of computing time; second, the success of such a model offers a degree of physical insight into radiative transfer in a clumpy medium.

REFERENCES

Abgrall, H., Le Bourlot, J., Pineau des Forets, G., Roueff, E., Flower, D. R., & Heck, L. 1992, A&A, 253, 525
Bakes, E. L. O., & Tielens, A. G. G. M. 1994, ApJ, 427, 822
Beresnyak, A., Lazarian, A., & Cho, J. 2005, ApJ, 624, L93
Bethell, T. J., Zweibel, E. G., Heitsch, F., & Mathis, J. S. 2004, ApJ, 610, 801 (B04)
Bethell, T. J., Zweibel, E. G., & Li, P. S. 2007, ApJ, submitted
Boissé, P. 1990, A&A, 228, 483
Calzetti, D., Bohlin, R. C., Gordon, K. D., Witt, A. N., & Bianchi, L. 1995, ApJ, 446, L97
Cardelli, J. A., Clayton, G. C., & Mathis, J. S. 1989, ApJ, 345, 245
Caselli, P., & Walmsley, C. M. 2001, in ASP Conf. Ser. 243, From Darkness to Light: Origin and Evolution of Young Stellar Clusters, ed. T. Montmerle & P. André (San Francisco: ASP), 67
Cecchi-Pestellini, C., Aiello, S., & Barsella, B. 1995, MNRAS, 274, 134
Chieze, J.-P., Pineau des Forets, G., & Herbst, E. 1991, ApJ, 373, 110
Code, A. D., & Whitney, B. A. 1995, ApJ, 441, 400
Deshpande, A. A. 2000, MNRAS, 317, 199
Draine, B. T. 1978, ApJS, 36, 595
———. 2003, ApJ, 598, 1017
Draine, B. T., & Bertoldi, F. 1996, ApJ, 468, 269

Elmegreen, B. G., & Scalo, J. 2004, ARA&A, 42, 211
Evans, N. J., II. 1999, ARA&A, 37, 311
Evans, N. J., II, Rawlings, J. M. C., Shirley, Y. L., & Mundy, L. G. 2001, ApJ, 557, 193
Faison, M. D., & Goss, W. M. 2001, AJ, 121, 2706
Flannery, B. P., Roberge, W., & Rybicki, G. B. 1980, ApJ, 236, 598
Garrod, R. T., Williams, D. A., Hartquist, T. W., Rawlings, J. M. C., & Viti, S. 2005, MNRAS, 356, 654
Gordon, K. D. 2004, in ASP Conf. Ser. 309, Astrophysics of Dust, ed. A. N. Witt, G. C. Clayton, & B. T. Draine (San Francisco: ASP), 77
Hegmann, M., & Kegel, W. H. 1996, MNRAS, 283, 167
Heiles, C. 1997, ApJ, 481, 193
Henyey, L. G., & Greenstein, J. L. 1941, ApJ, 93, 70
Hobson, M. P., & Padman, R. 1993, MNRAS, 264, 161
Hobson, M. P., & Scheuer, P. A. G. 1993, MNRAS, 264, 145
Hollenbach, D. J., & Tielens, A. G. G. M. 1997, ARA&A, 35, 179
———. 1999, Rev. Mod. Phys., 71, 173
Jansen, D. J., van Dishoeck, E. F., Black, J. H., Spaans, M., & Sosin, C. 1995, A&A, 302, 223
Juvela, M. 2005, A&A, 440, 531
Kramer, C., Stutzki, J., Rohrig, R., & Corneliussen, U. 1998, A&A, 329, 249
Lee, H.-H., Bettens, R. P. A., & Herbst, E. 1996, A&AS, 119, 111
Li, P. S., Norman, M. L., Mac Low, M.-M., & Heitsch, F. 2004, ApJ, 605, 800
Lillie, C. F., & Witt, A. N. 1976, ApJ, 208, 64
Mac Low, M.-M., & Klessen, R. S. 2004, Rev. Mod. Phys., 76, 125
Martin, H. M., Hills, R. E., & Sanders, D. B. 1984, MNRAS, 208, 35
Mathis, J. S. 1990, ARA&A, 28, 37
Mathis, J. S., Mezger, P. G., & Panagia, N. 1983, A&A, 128, 212 (MMP)
Mathis, J. S., Whitney, B. A., & Wood, K. 2002, ApJ, 574, 812
McKee, C. F. 1989, ApJ, 345, 782
Meixner, M., & Tielens, A. G. G. M. 1993, ApJ, 405, 216
Mouschovias, T. C., Tassis, K., & Kunz, M. W. 2006, ApJ, 646, 1043
Padoan, P., Willacy, K., Langer, W., & Juvela, M. 2004, ApJ, 614, 203
Perault, M., Falgarone, F., & Puget, J. L. 1985, A&A, 152, 371
Prasad, S. S., & Tarafdar, S. P. 1983, ApJ, 267, 603
Roberge, W. G., Dalgarno, A., & Flannery, B. P. 1981, ApJ, 243, 817
Sasseen, T. P., & Deharveng, J.-M. 1996, ApJ, 469, 691
Schnee, S., Bethell, T., & Goodman, A. 2006, ApJ, 640, L47
Spaans, M. 1996, A&A, 307, 271
Spaans, M., & Neufeld, D. A. 1997, ApJ, 484, 785
Stutzki, J., & Güsten, R. 1990, ApJ, 356, 513
Stutzki, J., Stacey, G. J., Genzel, R., Harris, A. I., Jaffe, D. T., & Lugten, J. B. 1988, ApJ, 332, 379
Sujatha, N. V., Shalima, P., Murthy, J., & Henry, R. C. 2005, ApJ, 633, 257
Verner, D. A., Ferland, G. J., Korista, K. T., & Yakovlev, D. G. 1996, ApJ, 465, 487
Weingartner, J. C., & Draine, B. T. 2001, ApJ, 563, 842
Williams, J. P., Bergin, E. A., Caselli, P., Myers, P. C., & Plume, R. 1998, ApJ, 503, 689
Witt, A. N. 1977, ApJS, 35, 1
Witt, A. N., & Gordon, K. D. 1996, ApJ, 463, 681
Witt, A. N., Oliveri, M. V., & Schild, R. E. 1990, AJ, 99, 888
Wood, K., Haffner, L. M., Reynolds, R. J., Mathis, J. S., & Madsen, G. 2005, ApJ, 633, 295
Zuckerman, B., & Evans, N. J., II. 1974, ApJ, 192, L149